THE ASTROPHYSICAL JOURNAL, 458:120–131, 1996 February 10

THE MOST COMPLETELY SAMPLED ROTATION CURVES FOR GALAXIES

YOSHIAKI SOFUE
Institute of Astronomy, University of Tokyo, Mitaka, Tokyo 181, Japan; sofue@mtk.ioa.s.u-tokyo.ac.jp
Received 1995 January 3; accepted 1995 July 25

ABSTRACT

We have compiled high-resolution position-velocity diagrams observed along the major axes of nearby spiral galaxies in the CO line emission, and derived rotation curves for the inner regions of the galaxies. We have combined the inner rotation curves with the outer H I and optical rotation curves to obtain the total rotation curves. The inner rotation curves are characterized by a steep increase within a radius of a few hundred parsecs, indicating a compact massive concentration near the nucleus. We fit the obtained rotation curves for individual galaxies by a modified Miyamoto-Nagai potential by assuming existence of four mass components: a nuclear mass component with a scale radius of 100–150 pc and a mass of ~ 3–$5 \times 10^9\ M_\odot$; a central bulge of 0.5–1 kpc radius of mass $\sim 10^{10}\ M_\odot$; a disk with scale radius 5–7 kpc and thickness 0.5 kpc of mass ~ 1–$2 \times 10^{11}\ M_\odot$; and a massive halo of scale radius 15–20 kpc with a mass ~ 2–$3 \times 10^{11}\ M_\odot$. We discuss the implication of the nuclear compact mass component for the formation mechanism of multiple structures within the central bulge of a galaxy during its formation.

Subject headings: galaxies: ISM — galaxies: kinematics and dynamics

1. INTRODUCTION

The rotation curves of galaxies have been obtained by optical (Hα) and H I 21 cm line-emission observations along the major axes (Rubin, Ford, & Thonnard 1980, 1982). It is well known that the H I gas distribution generally shows depression in the region of the central few kiloparsecs (Bosma 1981; Rots et al. 1990), which has yielded an apparently solid rotation curve for the central region. Optical measurements are effected by the contamination of the bright blue light, which has also increased the uncertainty of the curve near the center. Moreover, because of the dust absorption in the gaseous disk, optical observations cannot be obtained of the central regions of highly tilted galaxies, whereas edge-on galaxies are most suitable for determining the rotation curves without ambiguity of correction for inclination.

On the other hand, the CO line emission is generally concentrated in the central region, so that rotation curves of the inner few kiloparsecs can be most accurately obtained by CO position-velocity (PV) diagrams (Kenney & Young 1988; Young & Scoville 1992; Sofue & Nakai 1993; Sofue & Nakai 1994). It has been shown that the CO rotation curves of edge-on galaxies do not necessarily coincide with those obtained by H I and/or optical observations. The central rotation shown by CO is much flatter than that from H I and optical data, or even increases near the center, exhibiting a rapidly rotating compact disk component (Sofue & Nakai 1993, 1994; Sofue, Honma, & Arimoto 1994).

In this paper, we compile CO line PV diagrams along the major axes of nearby late-type (Sb and Sc) galaxies observed with large-aperture telescopes and interferometers. In particular, we extensively use CO line data from the Nobeyama Radio Observatory (NRO) 45 m telescope with an angular resolutions of 15″. We then deduce inner rotation curves from the CO PV diagrams, and combine them with outer H I and optical rotation curves to obtain the most completely sampled rotation curves. Of course, this technique of deducing the inner rotation curve works when nuclear CO is present: significant quantities of nuclear CO might not be universal. We further fit the obtained curves with the potential of Miyamoto & Nagai (1975) by assuming four mass components: a nuclear compact mass, bulge, disk, and a massive halo.

2. CO + H I POSITION-VELOCITY DIAGRAMS AND ROTATION CURVES

2.1. *Deriving Rotation Curves*

2.1.1. *Edge-on Galaxies*

Given a PV diagram along the major axis of an edge-on galaxy, the rotation curve can be derived by using the loci of terminal velocity (V_t) in the PV diagram. The terminal velocity is defined in a similar manner to that adopted for H I and CO line PV diagrams of our Galaxy (e.g., Clemens 1985). Thereby, the velocity dispersion of the interstellar gas ($\sigma_{\rm ISM}$) and the velocity resolution of observations ($\sigma_{\rm obs}$) must be corrected by

$$V_{\rm rot} = V_t - (\sigma_{\rm obs}^2 + \sigma_{\rm ISM}^2)^{1/2} . \quad (1)$$

For galaxies discussed in this paper, the velocity resolution was usually $\sigma_{\rm obs} \sim 10$ km s^{-1}. We take the same interstellar velocity dispersion as for molecular gas in our Galaxy, $\sigma_{\rm ISM} \sim 7$ km s^{-1} (Stark & Brand 1989; Malhotra 1994). In this paper, we adopted a correction for the velocity dispersion and velocity resolution of $V_{\rm rot} \simeq V_t - 12$ km s^{-1}. The accuracy of measuring the terminal velocity as below using PV diagrams was typically ± 10 km s^{-1}. So the accuracy of determining rotation velocities is not strongly dependent on the values of the velocity dispersion and resolution.

The terminal velocity is defined by a velocity at which the intensity becomes equal to

$$I_t = [(0.2 I_{\rm max})^2 + I_{\rm lc}^2]^{1/2} \quad (2)$$

on observed PV diagrams, where $I_{\rm max}$ and $I_{\rm lc}$ are the maximum intensity and intensity corresponding to the lowest contour level, respectively. This equation defines a 20% level of the intensity profile at a fixed position, $I_t \simeq 0.2 I_{\rm max}$, if the signal-to-noise ratio is sufficiently high. On the other hand, if the intensity is not strong enough, the equation gives $I_t \simeq I_{\rm lc}$, which approximately defines the loci along the lowest contour level (usually $\sim 3 \times$ rms noise).

We comment that rotation curves traced in this way may not represent those corresponding to physically identical positions in galaxies, since different galaxies have different CO/H I intensities, and, also, their observational data are of different sensitivities and linear resolutions. A threshold column density, instead of the above criterion, might be a possible alternative. However, it is impractical to apply it to different galaxies with different observational resolutions and sensitivities. Hence, the practical and probably most reliable way to derive the rotation curves using radio PV diagrams is the method described above. Obviously, the result is a limited observation (spatial and velocity resolutions and sensitivity) which depends on the proper line intensities of individual galaxies.

Figure 1 shows an example of a composite PV diagram for NGC 891 reproduced from Sofue & Nakai (1994). The CO gas is concentrated in the central region, while H I is distributed in the outer disk, having a void in the central region. In Figure 1 we superpose the obtained rotation curve for NGC 891 as an example. The H I gas indicates the rotation of the outer disk, whereas the CO emission indicates the rotation in the innermost region, including the rapidly rotating nuclear disk. The rotation curve as a function of the radius can be obtained by averaging and smoothing the absolute rotation velocities on both sides of the galaxy nucleus. The final rotation curves are then smoothed according to the angular resolution. The clumpy and smaller scale structures, which are due partly to clumpy ISM distributions and molecular clouds and partly to noise in the observations, are also smoothed by hand in drawing the final rotation curve.

In the following subsections, we derive rotation curves for individual galaxies. Generally, the rotation curves are almost flat, even in the very inner region, much flatter than those obtained from H I or optical observations. We describe individual galaxies below and summarize the observational parameters and references in Table 1.

2.1.2. *Mildly Tilted Galaxies*

For nearly face-on galaxies that have been observed with a sufficiently high angular resolution (e.g., sharper than several tens of parsecs), this method will give an almost identical rotation curve to that obtained by tracing intensity-weighted averages (e.g., using a velocity field map) which automatically account for the gas dispersion and velocity resolution. However, except for such an ideal case, both the finite beam and the disk thickness along the line of sight cause confusion of gases with smaller velocities than the terminal velocity, and both would result in a lower rotation velocity. Hence, even for mildly tilted galaxies observed with a finite beamwidth, we use PV diagrams along the major axes and apply the same method as for edge-on galaxies.

2.1.3. *Innermost Rotation Curves*

This envelope-tracing technique encounters difficulty when applied to the innermost part of the PV diagram, since simply traced envelopes on the two sides of the nucleus have a discontinuity at the nucleus due mainly to the finite beamwidth. We have avoided this discontinuity by stopping the tracing at a radius corresponding to the telescope resolution and then connecting both sides of the rotation curve by a straight (solid-body–like) line crossing the nucleus at zero velocity. Therefore, the resolution of an obtained rotation curve is limited by the angular resolution of the observation.

The inner rotation curves are determined by CO data, while those in the outer disk are determined from H I and optical data. When we used data from different observations, we adopted higher resolution data. The data are then smoothly connected by tracing higher velocity parts. Note that CO data usually have higher resolution than H I. When comparable data were present in the same region, we simply averaged them.

2.2. *Rotation Curves for Individual Galaxies*

We present the obtained rotation curves for individual galaxies. Basic parameters such as the distance and references for individual galaxies are given in Table 1.

2.2.1. *NGC 253*

For its proximity at a distance of 2.5 Mpc (Pence 1980), relatively low-resolution CO data obtained with the FCRAO 14 m telescope (Scoville et al. 1985) could resolve the central

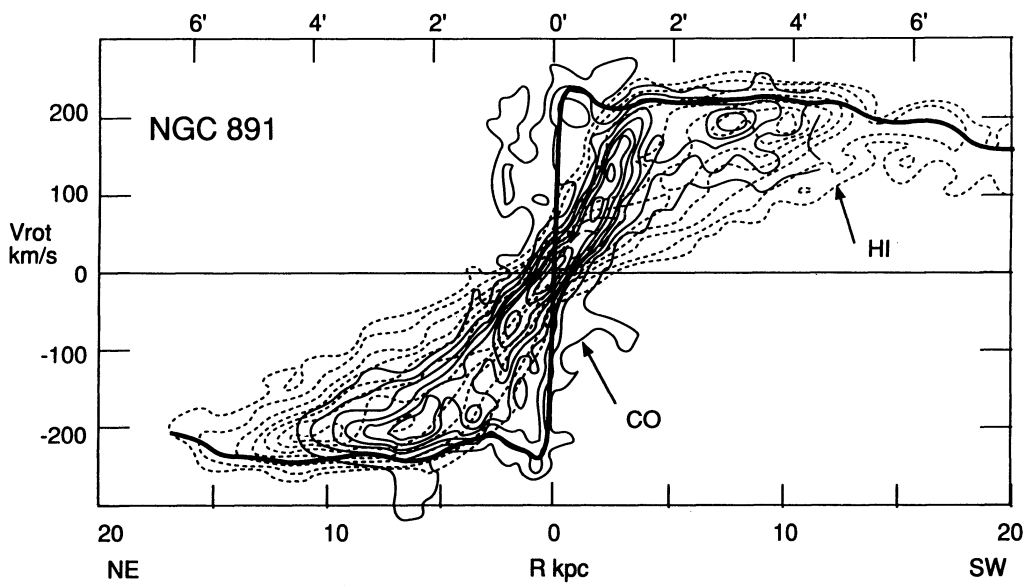

FIG. 1.—CO + H I composite position-velocity diagram for NGC 891 as reproduced from Sofue et al. (1994). A rotation curve is superposed by the thick line.

TABLE 1

PARAMETERS FOR GALAXIES AND REFERENCES FOR PV DIAGRAMS AND ROTATION CURVES

Galaxy	Type	Inclination	Distance[a] (Mpc)	Line	Angular Resolution	Linear Resolution (kpc)	References
NGC 253	Sc	78°.5	2.5	CO	45″	0.55	Scoville et al. 1985
				Hα	...	...	Pence 1980
				H I	120	1.5	Combes et al. 1977
IC 342	Sc	25	3.9	CO	15	0.28	Hayashi et al. 1987
				CO	4	0.076	Ishizuki et al. 1990a
				CO	45	0.85	Young & Scoville 1982
				CO	45	0.85	Sage & Solomon 1991
				H I	50	0.9	Rogstad & Shostak 1972
NGC 891	Sb	88.3	8.9	CO	4	0.17	Scoville et al. 1993
				CO(2–1)	13	0.55	Garcia-Burillo et al. 1992
				CO	15	0.65	Sofue & Nakai 1993
				H I	20	0.86	Rupen 1991
NGC 1808	Sbc	58	11.4	CO	15	0.83	Sofue 1994, private communication
				CO	45	2.40	Dahlem et al. 1990
				H I	20	1.1	Saikia et al. 1990
				H I	20	1.1	Koribalski et al. 1993
NGC 3079	Sc	~90	15.6	CO	4	0.30	Sofue & Irwin 1992
				CO	45	3.4	Young, Claussen, & Scoville 1988
				H I	20	0.15	Irwin & Seaquist 1991
NGC 4565	Sb	86	10.2	CO	15	0.74	Sofue & Nakai 1993
				H I	20	1.0	Rupen 1991
NGC 5194 (M51)	Sc	20	9.6	CO(2–1)	13	0.60	Garcia-Burillo et al. 1993
				Hα	...	...	Tully 1974
				H I	20	1	Rots et al. 1990
NGC 5907	Sc	88	11.6	CO	15	0.84	Sofue 1994
				CO(2–1)	13	0.7	Garcia-Burillo & Guelin 1995
				H I	40	2.2	Casertano 1983
NGC 6946	Sc	30	5.5	CO	4	0.11	Ishizuki et al. 1990b
				CO	15	0.40	Sofue et al. 1988
				CO(2–1)	13	0.35	Casoli et al. 1990
				H I	20	0.5	Tacconi & Young 1986
				H I	50	0.9	Rogstad & Shostak 1972
Galaxy	Sb	90	0	CO, H I, H II	...	...	Clemens 1985

[a] REFERENCES TO DISTANCES.—NGC 253, Pence 1980; IC 342, Tully 1988; NGC 891, Handa et al. 1992; NGC 1808, Galactocentric velocity 856 km s^{-1}, $H_0 = 75$ km s^{-1} Mpc^{-1}; NGC 3079, Sofue & Irwin 1992; NGC 4565, Schöniger & Sofue 1993; NGC 5194, Sandage & Tammann 1974; NGC 5907, Schöniger & Sofue 1993; NGC 6946, Tully 1988.

molecular disk at a linear resolution of 45″ = 545 pc. A PV diagram obtained by Scoville et al. (1985) indicates a steep increase of the rotation velocity near the nucleus within $R \sim 0.3$ kpc. An optical rotation curve has been obtained by Pence (1980), which indicates a flat rotation at 2–5 kpc radius. More outer-rotation characteristics can be derived from an H I velocity field observed by Combes, Gottesman, & Weliachew (1977).

By combining rotation curves derived from these diagrams, which are shown in Figure 2*a*, we constructed a total rotation curve as shown in Figure 2*b*, where the inclination of $i = 78°.5$ has been corrected. Hereafter, panels *a* and *b* in each figure will show curves fitted to data and the resultant rotation curve, respectively. The rotation velocity increases steeply in the central region and attains a maximum of 210 km s^{-1} at $R \sim 0.3$ kpc. Then the curve is almost perfectly flat until $R \sim 9$ kpc.

2.2.2. *IC 342*

This is an almost face-on ($i = 25°$) Sc galaxy at 3.9 Mpc distance. It has been extensively studied in the CO line, and various PV diagrams have been obtained (Young & Scoville 1982; Hayashi et al. 1987; Sage & Solomon 1991). A rotation curve in the H I line has been obtained by Rogstad & Shostak (1972). In this paper, we make use of PV diagrams observed with the NRO 45 m telescope at a resolution of 15″ (284 pc; Hayashi et al. 1987) and a 4″ resolution millimeter array PV diagram (Ishizuki et al. 1990a; Ishizuki 1994, private communication). Figure 3 shows the obtained rotation curve for IC 342 using the PV diagrams.

The rotation velocity increases almost rigidly in the innermost region at $R < 10″ = 190$ pc, and reaches $V_{rot} \sim 130$ km s^{-1} at $R \sim 15″$ (280 pc). Then it increases gradually to reach a maximum of 190 km s^{-1} at $R \sim 2'$–$3'$ (2–3 kpc), followed by a flat H I rotation at 195 km s^{-1} (at 8 kpc) to 190 km s^{-1} (at 20 kpc).

2.2.3. *NGC 891*

This edge-on Sb galaxy at a distance of 8.9 Mpc has been extensively observed in the CO line using the IRAM 30 m telescope (Garcia-Burillo et al. 1992), the NRO 45 m telescope (Sofue & Nakai 1993), and the Owens Valley Radio Observatory (OVRO) interferometer (Scoville et al. 1993). It has been mapped in the H I line (Sancisi 1976a; Rupen 1991) at a comparable resolution to the CO observations. In Figure 1 we show a composite PV diagram of the CO and H I lines reproduced from Sofue et al. (1994). The CO diagram is characterized by the 4 kpc molecular ring and the high-velocity nuclear disk at $R < 1$ kpc. The H I gas is distributed in a broad ring and outskirts at $R > 10$ kpc. For deriving the rotation curve near the nucleus, we also made use of the IRAM CO ($J = 2$–1) observation at a 13″ resolution (Garcia-Burillo et al. 1992) and the higher resolution PV diagram obtained by interferometer observations by Scoville et al. (1993).

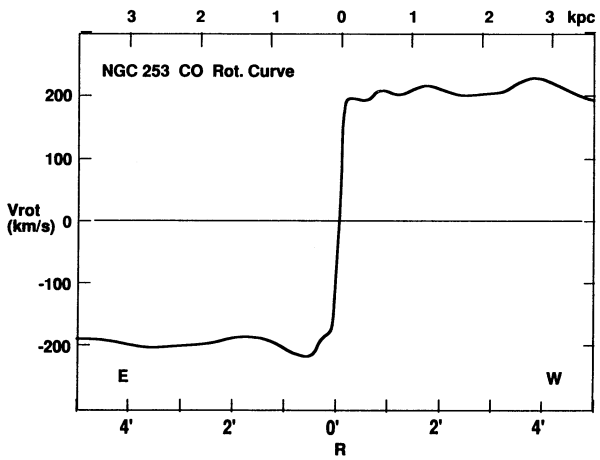

FIG. 2*a*-1

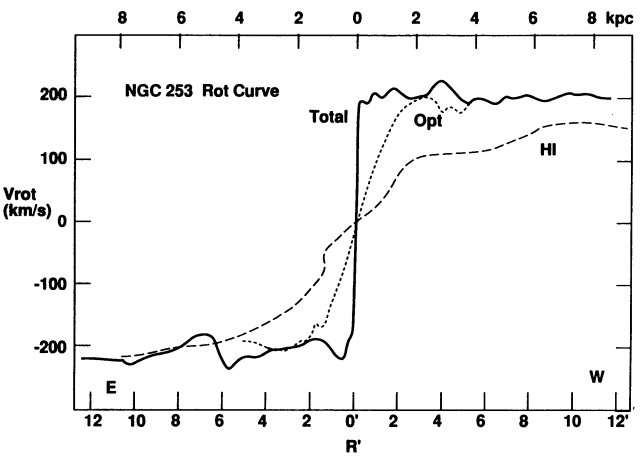

FIG. 2*a*-2

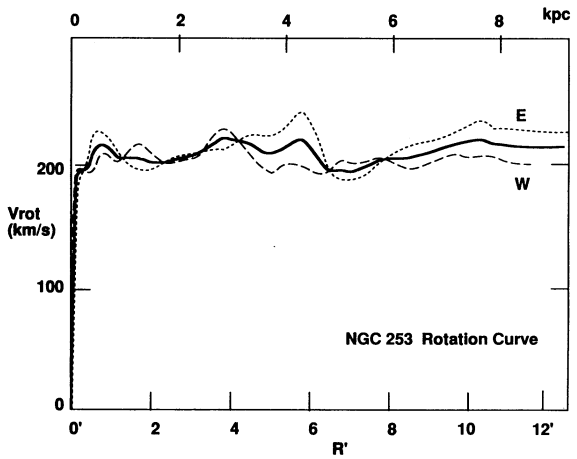

FIG. 2*b*

FIG. 2.—(*a*-1) Inner rotation curve of NGC 253 derived by using the CO PV diagram, and (*a*-2) CO + optical (Hα) (= total) rotation curve compared to H I rotation. (*b*) Total rotation curve of NGC 253 obtained by averaging and smoothing the eastern and western halves of the rotation velocities. See Table 1 for observational parameters and references.

The obtained rotation curve is given in Figure 4. After a steep rise near the nucleus, the rotation velocity attains a steep maximum over 250 km s^{-1}, followed by a dip at $R = 2$ kpc. Then it becomes almost flat at $R \sim 3$ kpc and remains so until $R \sim 15$ kpc. Beyond this radius, the rotation velocity gradually declines toward the outermost region. The rotation curve is very similar to that of our Galaxy (Fig. 11).

2.2.4. *NGC 1808*

NGC 1808 is an Sbc galaxy known for its dusty jet (Véron-Cetty & Véron 1985), and the distance is 11.4 Mpc for a Hubble constant of 75 km s^{-1} Mpc^{-1}, and the inclination angle is $i = 58°$. H I observations using the VLA (Saikia et al. 1990) indicated a circular rotation ring of $\sim$7 kpc radius. Koribalski, Dickey, & Mebold (1993) performed a mapping of the H I line absorption in the nuclear region using the VLA and found a nuclear ring of cold, dense rotating gas of radius 500 pc. Dahlem et al. (1990) used the Swedish ESO Submillimeter Telescope (SEST) 15 m telescope to map NGC 1808 in the CO line emission at an angular resolution of 43″, revealing a central condensation of molecular gas. We have mapped the central 1′ region using the NRO 45 m telescope at a resolution of 15″ in the CO emission and obtained a high-resolution PV diagram along the major axis. This diagram shows a high-velocity rotating nuclear disk, consistent with the result of Koribalski et al. (1993). The H I and CO PV diagrams have been used to construct a rotation curve as shown in Figure 5. The rotation speed increases steeply to 210 km s^{-1} at $R \sim 10''$ (500 pc) in the nuclear region and then decreases to 190 km s^{-1} at $R \sim 3$ kpc. It increases again to a maximum of 210 km s^{-1} at $R \sim 2'$ (7 kpc) in the H I rotation curve. Beyond this radius, the rotation declines to $V_{rot} \sim 130$ km s^{-1} at $R \sim 6'$ (18 kpc). Such a declining rotation in the outskirts is rather exceptional among the galaxies studied here, except M51 outskirts, suggesting a small-mass massive halo.

2.2.5. *NGC 3079*

This is an amorphous edge-on galaxy classified as Sc type, showing an anomalously high concentration of CO gas in the center (Sofue et al. 1994). The distance is taken to be 15.6 Mpc using the H I systemic velocity and a Hubble constant of $H_0 =$ 75 km s^{-1} Mpc^{-1} (Sofue & Irwin 1992). Figure 6 shows the rotation curve produced by using the composite CO + H I PV diagram obtained by Sofue et al. (1994). Here they used a VLA H I PV diagram from Irwin & Seaquist (1991) and CO data from the Nobeyama Millimeter Array (NMA) (Sofue & Irwin 1992). This galaxy exhibits an exceptionally high concentration of CO emission in the galactic center. This high-density nuclear disk is clearly visible as the absorption feature in the H I line.

The rotation velocity shows a steep rise to a maximum as high as 320 km s^{-1} on the southeast side and 260 km s^{-1} on the northwest, followed by a dip at a few kiloparsec radius. The rotation velocity of this nuclear disk component is highly asymmetric with respect to the nucleus. The asymmetric rotation continues until $r \sim 8$ kpc. The H I gas is widely distributed in the broad ring at $R = 1'$–$2'$ (5–10 kpc) and in the outskirts showing a symmetric flat rotation.

2.2.6. *NGC 4565*

This is an almost edge-on ($i = 86°$) Sb galaxy at a distance of 10.2 Mpc. A CO + H I composite PV diagram similar to Figure 1 has been obtained by Sofue et al. (1994), who used CO data from NRO (Sofue & Nakai 1994) and H I from the VLA (Rupen 1991). The CO PV diagram shows a significant asymmetry in the intensity distribution: the CO emission in the southeast few kiloparsec region is very weak, so that the CO rotation in this region is not clear. However, except for this

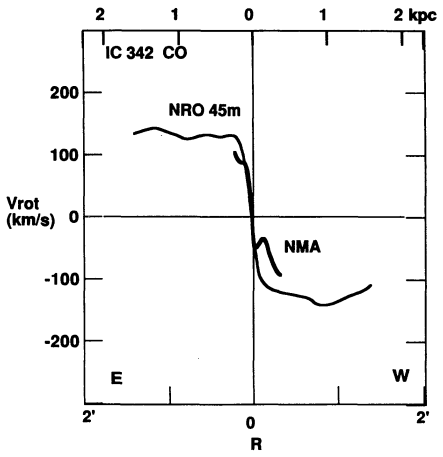

FIG. 3a-1

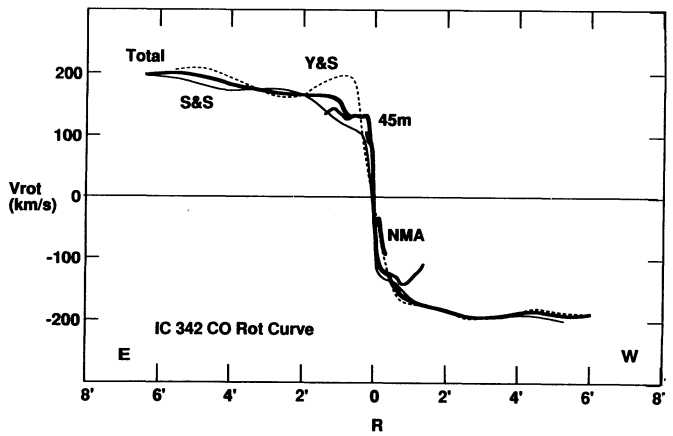

FIG. 3a-2

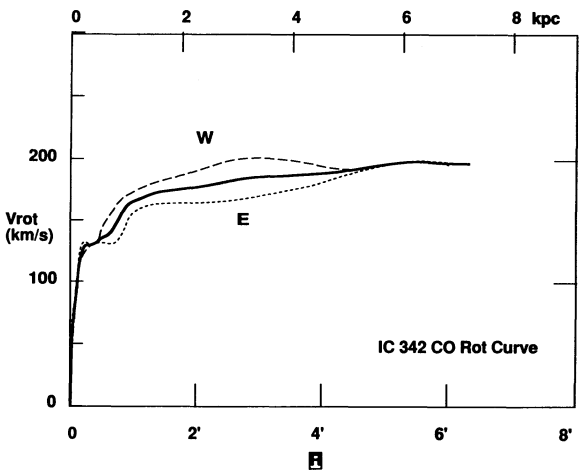

FIG. 3a-3

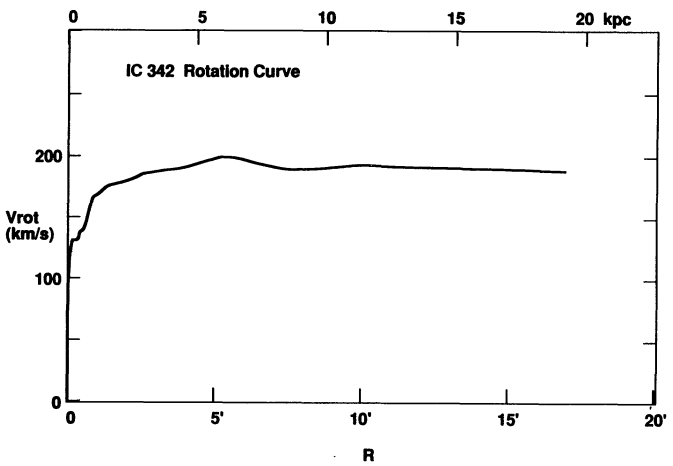

FIG. 3b

FIG. 3.—(*a*-1) CO rotation curves for IC 342 obtained by NRO 45 m telescope and the millimeter wave array. (*a*-2) CO rotation curves obtained by lower resolution observations compared to those in (*a*-1). (*a*-3) CO rotation curve obtained using curves in (*a*-1) and (*a*-2). (*b*) Total rotation curve of IC 342 obtained by combining and smoothing the CO curves with H I curve.

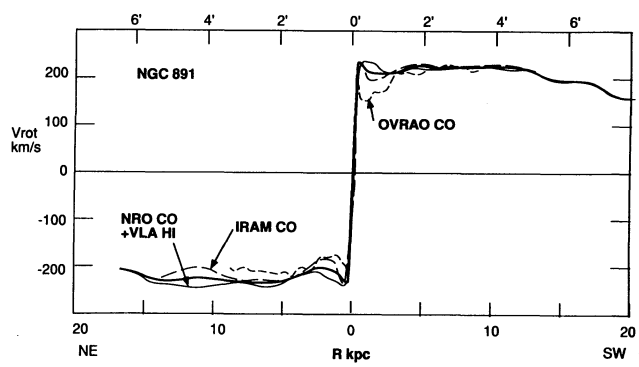

FIG. 4a

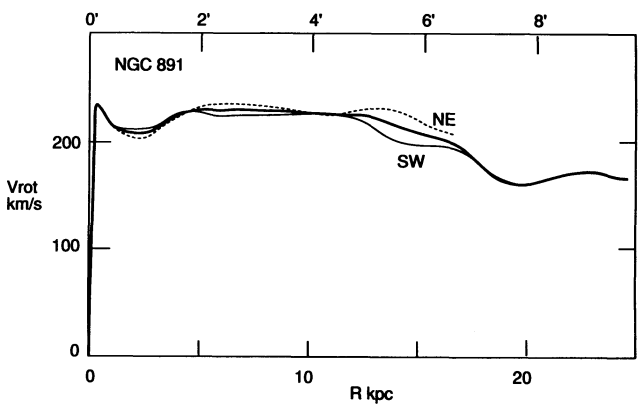

FIG. 4b

FIG. 4.—(*a*) CO and H I rotation curves for NGC 891 shown separately for the northeast and southwest part along the major axis. (*b*) Total rotation curve of NGC 891.

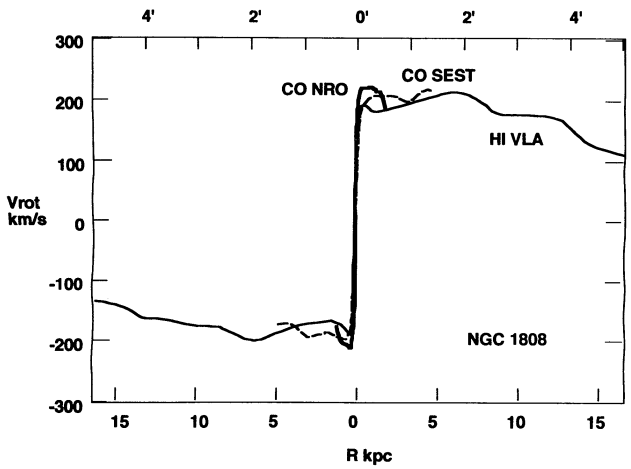

FIG. 5a

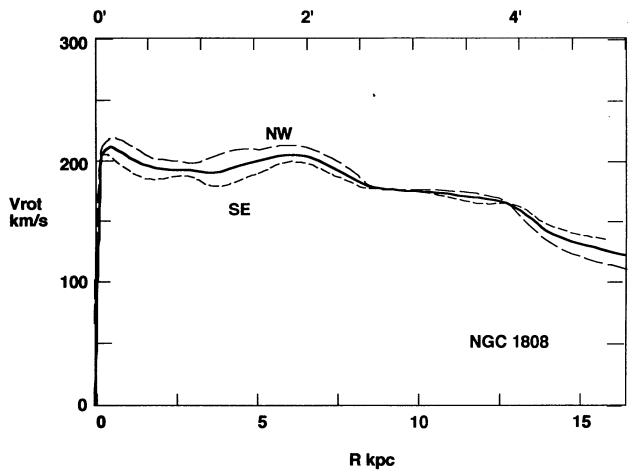

FIG. 5b

FIG. 5.—(*a*) CO and H I rotation curves for NGC 1808. (*b*) Total rotation curve.

region, the total rotation characteristics are almost symmetric and mimic those of NGC 891. On the other hand, the H I diagram shows an almost perfect symmetry in both intensity and rotation velocity.

The rotation curve as obtained from these diagrams is shown in Figure 7, which is similar to that for NGC 891. It has a nuclear-disk component rotating at 260 km s^{-1}, followed by a flat rotation until 20–25 kpc at a velocity as high as ~250 km s^{-1}. This galaxy is one of those with extremely flat rotation even in the outskirts, suggesting a large extended massive halo.

2.2.7. *NGC 5194 (M51)*

This nearly face-on Sbc galaxy at an inclination 20° and distance 9.6 Mpc has been extensively studied in all wavelengths. Tully (1974) derived a rotation curve from optical spectroscopic data for a wide area. Rots et al. (1990) have extensively mapped this galaxy in H I and obtained an intensity-averaged H I velocity field. However, they are not appropriate to derive an inner (a few kiloparsec) rotation curve, because the H I emission is very weak in the central region (Rots et al. 1990), so that the intensity-averaged velocity is significantly weighted by rotation velocity at larger radius. Unfortunately, no H I PV diagram has been obtained, as yet, along the major axis. A high-resolution CO PV diagram has been obtained by Garcia-Burillo, Guélin, & Cernicharo (1993) and Nakai et al. (1994). Here we use the CO PV diagram by Garcia-Burillo et al. (1993). The outer rotation curve can also be obtained by the H I velocity field, which agrees with that obtained from the CO data.

After correcting for the inclination of $i = 20°$, we obtained a CO and an Hα rotation curve as shown in Figure 8*a*. The CO rotation velocity at $R < \sim 5$ kpc is significantly higher than that from the Hα velocity. This may be due to the fact that the density wave velocity jump in the arms of M51 is as high as ~50 km s^{-1}, which would cause a systematic velocity difference of CO-emitting regions (dark lanes) from star-forming regions (OB stellar arms) (Nakai et al. 1995, in preparation). According to the definition of a rotation curve, we simply adopt the highest velocities (terminal velocities) along the major axis. Hence, most of the final rotation curve obtained in Figure 8*b* coincides with the CO rotation curve. The rotation velocity increases steeply near the nucleus, within 0.5 kpc, reaching a maximum of 260 km s^{-1}. Then it remains flat up to 9 kpc, beyond which the rotation velocity declines to 130 km s^{-1} at $R \sim 15$ kpc. This declining rotation is similar to that observed in NGC 1808.

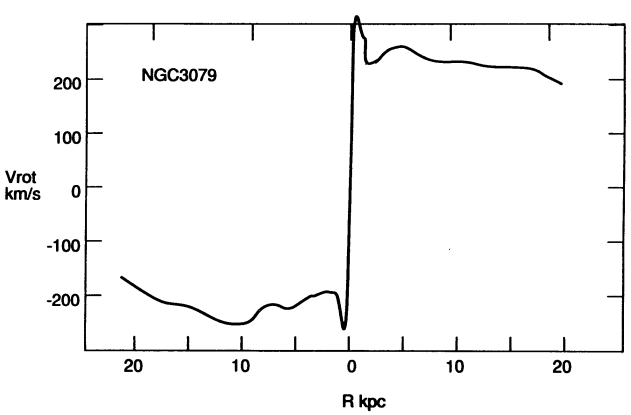

FIG. 6a

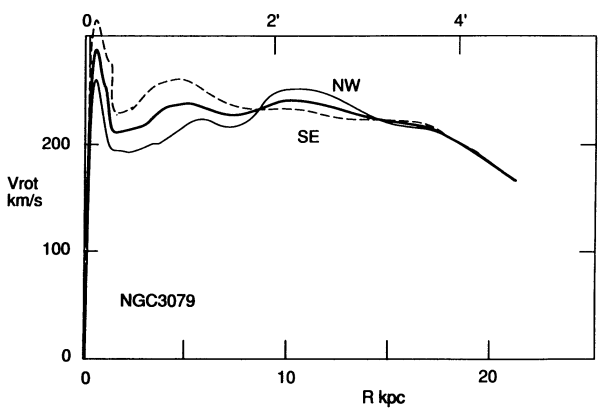

FIG. 6b

FIG. 6.—(*a*) CO and H I absorption rotation curves for the inner region combined with the H I rotation for the outer part. (*b*) Total rotation curve for NGC 3079.

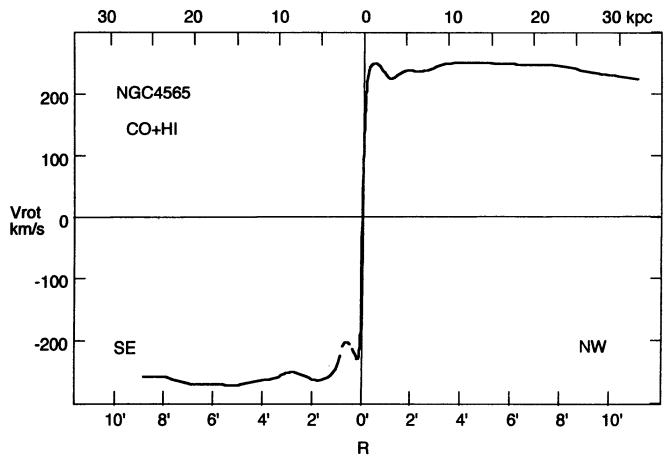

FIG. 7a

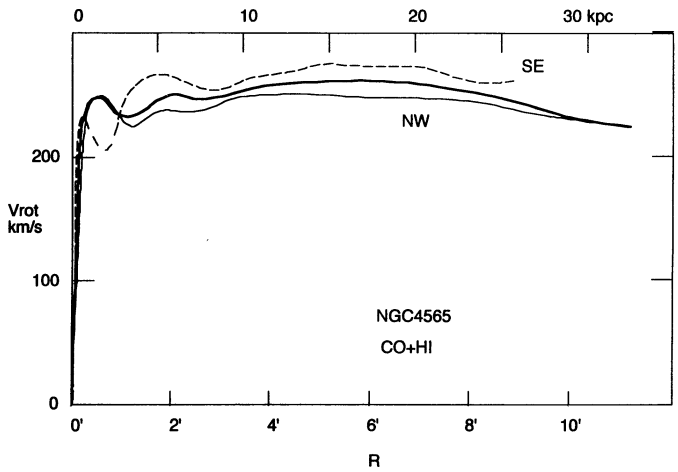

FIG. 7b

FIG. 7.—(*a*) Inner CO and outer H I rotation curves for NGC 4565. (*b*) Total rotation curve.

2.2.8. *NGC 5907*

NGC 5907 is a nearby Sc galaxy with an almost edge-on orientation at an inclination angle of 88°. Observations of the H I line emission have shown a large disk of interstellar gas, which is warping in the outermost regions (Sancisi 1976b). A CO + H I composite PV diagram for NGC 5907 has been obtained by Sofue et al. (1994), who used CO data from the NRO (Sofue 1994) and H I data from the Westerbork synthesis radio telescope (WSRT) (Casertano 1983). Recently, a nuclear disk component has been observed in the CO ($J = 2$–1) line with the IRAM 30 m telescope, which showed two symmetrical humps in the PV diagram at rotation velocities +200 and −190 km s^{-1} at 10″ to the northwest and southeast of the nucleus (Garcia-Burillo & Guélin 1995). This indicates that the rotation velocity increases steeply in the central ~10″ (500 pc). Unfortunately, the H I PV diagram has been obtained only for the southeast side, which we used to derive an H I total rotation curve, assuming that the rotation is axisymmetric. So, we first obtained the CO rotation curve at $R < 10$ kpc by averaging the southeast and northwest CO curves, and we obtained the final rotation curve in Figure 9*b* by smoothing the CO and H I total rotation curves. After the steep rising near the nucleus, the rotation curve is almost flat until 20 kpc, beyond which it gradually declines.

2.2.9. *NGC 6946*

This is a nearly face-on galaxy at a 5.5 Mpc distance and has been observed in high resolution in the CO line (Sofue et al. 1988; Ishizuki et al. 1990b; Casoli et al. 1990). Ishizuki et al. (1990b) have obtained a CO PV diagram using the NMA at a resolution of 4″, which showed a very steep rise of the rotation velocity up to a sharp maximum at 220–230 km s^{-1} within the central 2″ (53 pc). An inner rotation curve obtained from this PV diagram is shown in Figure 10*a*-1. Sofue et al. (1988) have obtained a wide-area rotation curve by combining CO data from the NRO 45 m observations with an H I rotation curve by Tacconi & Young (1986). They have shown that the rotation is almost perfectly flat from the very center to the outskirts at $R \sim 15$ kpc. Casoli et al. (1990) have combined the CO PV diagram from IRAM 30 m observations with an H I PV diagram, showing that the rotation is almost flat toward the center. We used this PV diagram to obtain the CO rotation curve shown in Figure 10*a*-2.

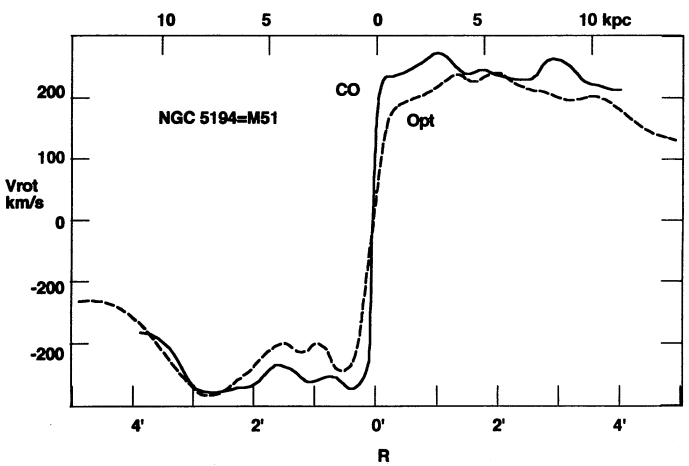

FIG. 8a

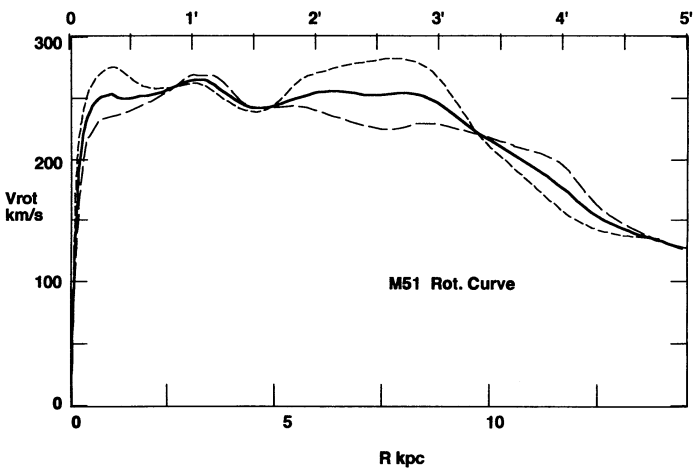

FIG. 8b

FIG. 8.—(*a*) CO and optical rotation curves for NGC 5194 (M51). (*b*) Total rotation curve of M51.

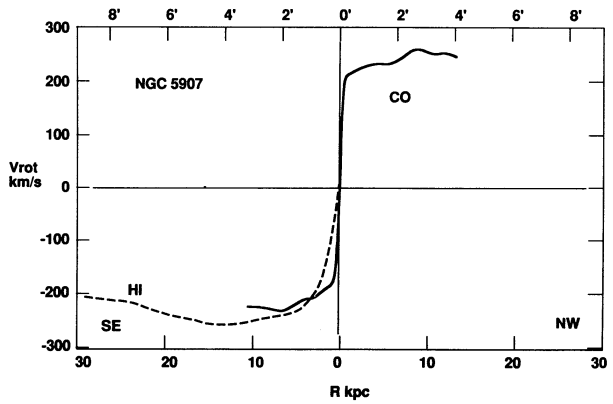

FIG. 9a

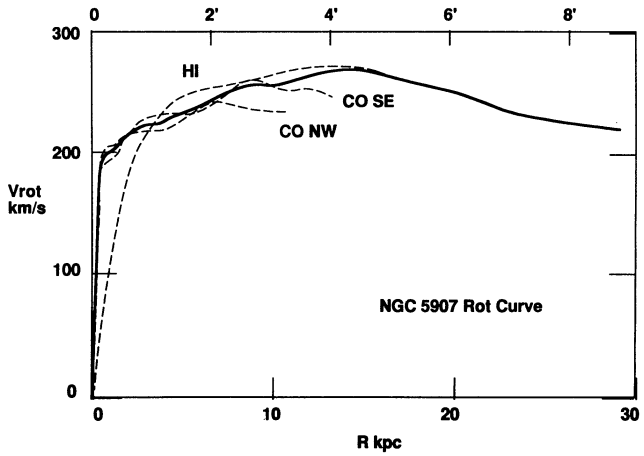

FIG. 9b

FIG. 9.—(*a*) CO + H I rotation curves for NGC 5907. (*b*) Total rotation curve.

We have combined all these rotation curves in Figures 10*a*-1 and 10*a*-2, and obtained a rotation curve as shown in Figures 10*a*-3 and 10*b*. Here we have corrected for the inclination of $i = 30°$. The steep rising near the nucleus is followed by a decrease to a dip at ~1 kpc, followed by a flat minimum at 185 km s^{-1} until 3 kpc. Then the rotation velocity gradually increases to attain 220 km s^{-1} at $R \sim 7$ kpc, beyond which the rotation is nearly flat. The flat rotation appears to continue until the observed edge of the galaxy at $R \sim 16$ kpc. The rotation curve mimics the one for our Galaxy, as shown in the next subsection.

2.3. *The Milky Way*

The Milky Way Galaxy has long been observed in both H I and CO, and many longitude-velocity (l-V_{lsr}) diagrams have

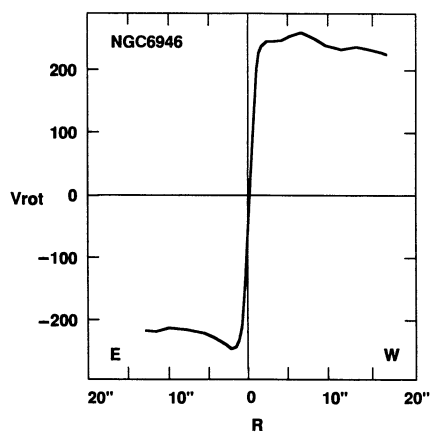

FIG. 10a-1

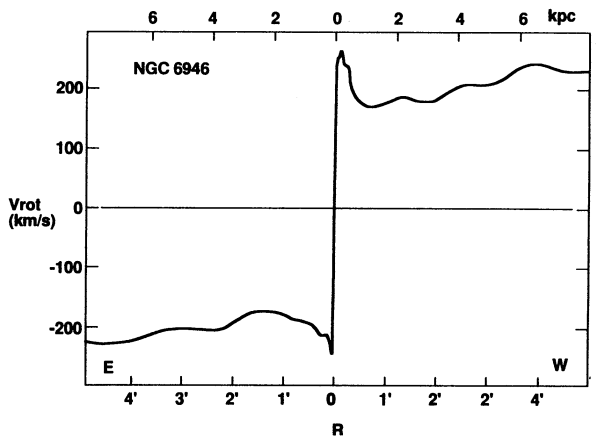

FIG. 10a-2

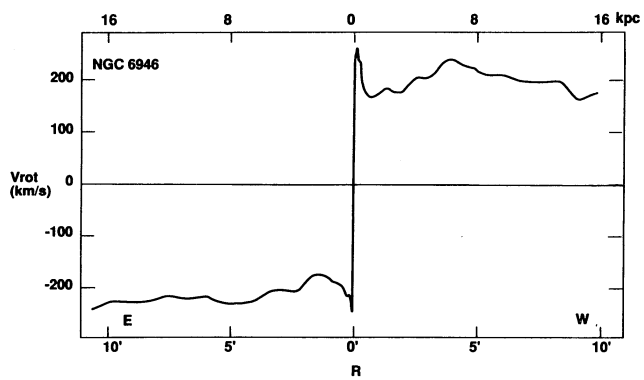

FIG. 10a-3

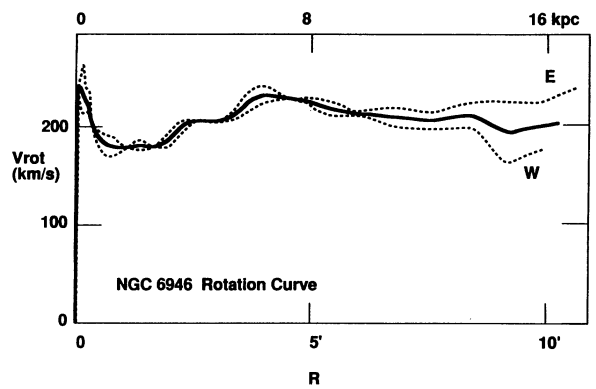

FIG. 10b

FIG. 10.—(*a*-1) CO rotation curve from the millimeter array for the nuclear region of NGC 6946, (*a*-2) CO rotation curves, and (*a*-3) CO + H I rotation curves. (*b*) Total rotation curve of NGC 6946.

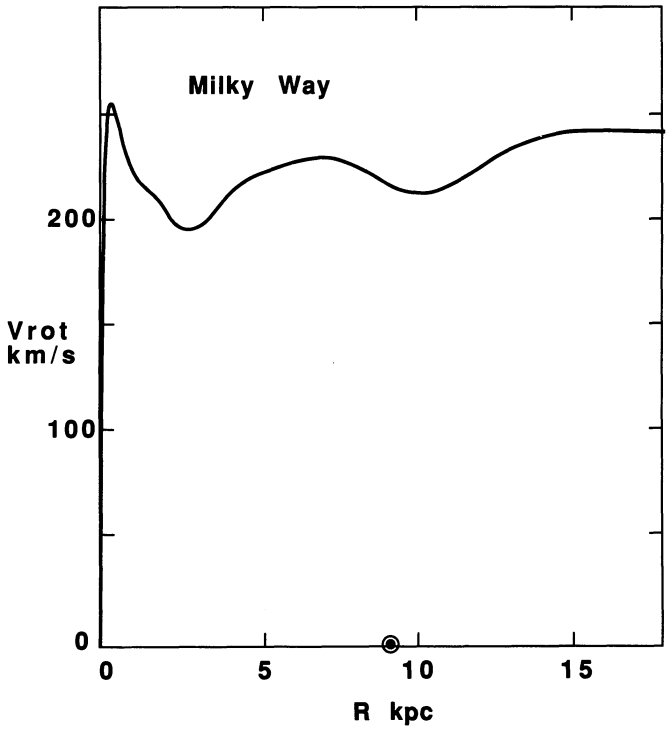

FIG. 11.—Rotation curve of our Galaxy reproduced from Clemens (1985)

been published. These diagrams have been used to obtain rotation curves of our Galaxy. Burton & Gordon (1978) obtained an H I rotation curve at a 0°.5 resolution for the Galactic disk within the solar circle and combined the H I data with CO data at $l > 8°$. Clemens (1985) has analyzed the ^{12}CO line survey data for $l > 13°$ and integrated all the existing rotation curves to present a total rotation curve of our Galaxy, including the outer disk of the solar circle. In these studies, the rotation of the central few degree region has been obtained by the terminal-velocity tracing method of the H I data (Burton & Gordon 1978). In Figure 11 we reproduce the total rotation curve derived by Clemens (1985). Here the solar rotation and radius are taken to be 220 km s^{-1} and 8.5 kpc, respectively.

2.4. *Comparison of Rotation Curves*

All the rotation curves obtained in this work are shown in the same scale in Figures 12*a* and 12*b*. Figure 12*a* shows the rotation curves with a steep central peak, while Figure 12*b* shows those without. Generally, the rotation velocity rises steeply within a few hundred parsecs, indicating the existence of a central compact mass component. Many galaxies (the Milky Way, NGC 891, NGC 3079, and NGC 6946) exhibit a sharp maximum at $R \sim$ a few hundred parsecs, reaching a velocity as high as $\sim$200–300 km s^{-1}. On the other hand, the maximum velocity corresponding to this component is not so high in such galaxies as NGC 253, IC 342, and M51, where the existence of the steep and sharp rise near the nucleus is also evident.

3. FITTING BY MIYAMOTO-NAGAI POTENTIAL

We try to fit the rotation curve by the Miyamoto-Nagai (1975) potential. A modified Miyamoto-Nagai potential, with n mass components, is expressed in (R, z) coordinates in the following equation. Here R denotes the distance from the rotation axis, and z is the height from the galactic plane.

$$\Phi = \sum_{i=1}^{n} \frac{GM_i}{\{R^2 + [a_i + (z^2 + b_i^2)^{1/2}]^2\}^{1/2}}, \quad (3)$$

where M_i, a_i, and b_i are the mass, scale radius, and scale thickness of the ith mass component of the galaxy. For a spherical mass distribution, we have $a_i = 0$, and b_i becomes equal to the scale radius of the sphere. The rotation velocity is calculated by

$$V_{\rm rot} = \left(R \frac{\partial \Phi}{\partial R} \right)^{1/2}. \quad (4)$$

Miyamoto & Nagai (1975) have assumed two components ($n = 2$). In order to fit the flat rotation at $R \sim$ 10–20 kpc, an extended massive halo has to be introduced. Since their model was proposed, a three-component model ($n = 3$) has been widely used, which assumes the central bulge, disk, and massive halo. However, after a trial of fitting to the rotation curves of the central few hundred parsecs region as obtained here, it turned out that the usual three-component model is not sufficient to fit the steep central peak. Therefore, in addition to the usual three components, we have introduced a fourth component which represents a more compact nuclear component.

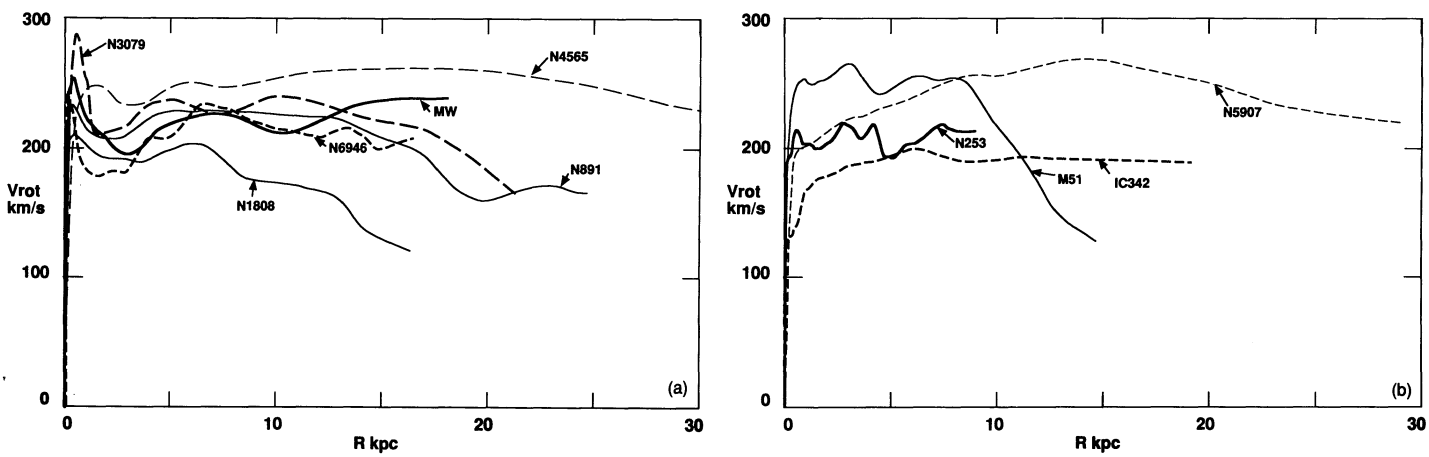

FIG. 12.—Rotation curves of galaxies studied in this paper plotted in the same linear and velocity scales. (*a*) Rotation curves having a central peak similar to that of our Galaxy. (*b*) Rotation curves without significant central peak.

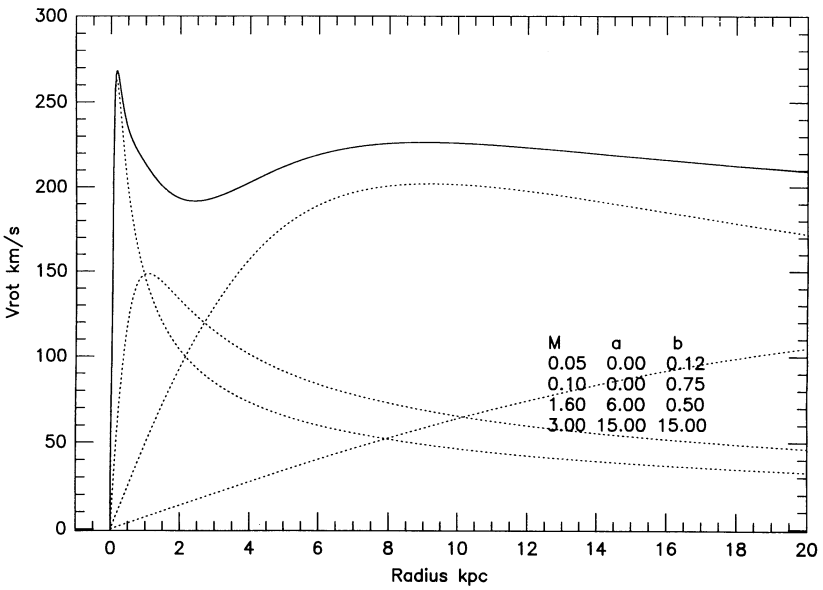

FIG. 13.—Model rotation curve of our Galaxy as calculated for the Miyamoto-Nagai potential with four components: (1) nuclear mass component, (2) bulge component with scale radius a few hundred parsecs, (3) disk components, and (4) massive halo component. The mass M in $10^{11}\ M_\odot$, scale radius a and the thickness b in kiloparsecs of each component are indicated by the inset table. Inset table shows the mass M in $10^{11}\ M_\odot$, scale radius a and thickness b in kiloparsecs for the four mass components of the modified Miyamoto-Nagai potential in eq. (3). Dashed lines indicate rotation velocities corresponding to each mass component.

Figure 13 shows an example of a calculated rotation curve of this "four-component" model ($n = 4$), where we assumed (1) a nuclear compact mass component, (2) bulge, (3) disk, and (4) a massive halo. The table inset in Figure 13 presents the parameter combination. Dashed lines indicate rotation curves corresponding to individual components. The rotation curve of our Galaxy, except for the central 10–50 pc, can be fitted by a model with (1) a nuclear mass of $M_1 = 5 \times 10^9\ M_\odot$ of a $b_1 =$ 120 pc scale radius, (2) the bulge of $M_2 = 10^{10}\ M_\odot$ and $b_2 =$ 750 pc radius, (3) the disk of $M_3 = 1.6 \times 10^{11}\ M_\odot$ with radius $a_3 = 6$ kpc and thickness $b_3 = 0.5$ kpc, and (4) a massive halo of $M_4 = 3 \times 10^{11}\ M_\odot$ and scale radius of $a_4 = b_4 = 15$ kpc. The rotation of NGC 891 can be reproduced by the same model with a similar parameter combination.

In this four-component model, however, the very inner rotation within a few tens of parsecs region of our Galaxy, as shown in Figure 11, cannot be reproduced. Since it is beyond the scope of the present paper to discuss a detailed nuclear mass distribution, we only argue for the necessity of introducing more central components. In order to fit the observed inner rotation curve, we need to add a fifth component at the nucleus with a smaller scale ($\sim$30 pc), radius, and mass ($\sim 10^7\ M_\odot$), and, as well, a central pointlike mass of a few times $10^6\ M_\odot$.

Similarly, the rotation curve observed for NGC 6946 is fitted by the model as shown in Figure 14. The flat valley at the $R \sim$ 1–2 kpc region, which was difficult to reproduce by the three-component model, can be fitted well by introducing the

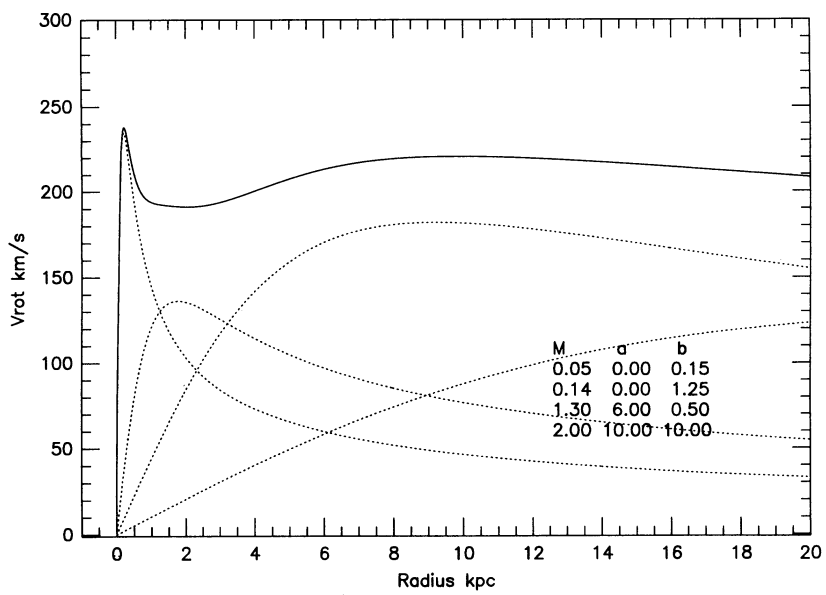

FIG. 14.—Same as Fig. 13, but mimicking curve for NGC 6946

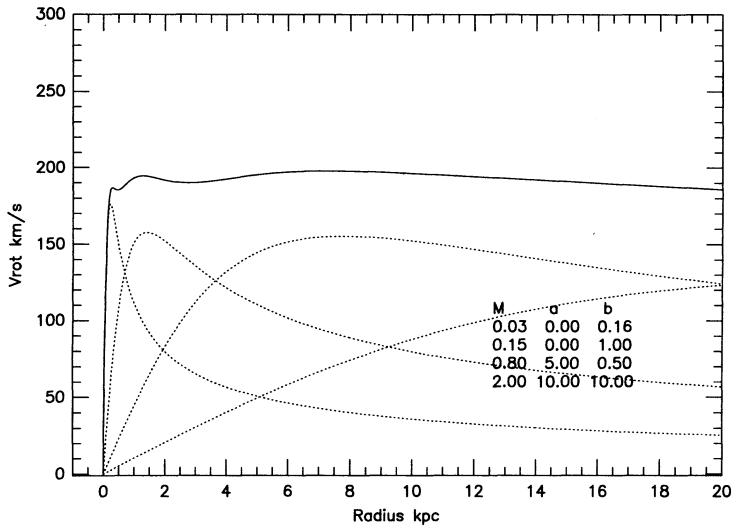

FIG. 15.—Same as Fig. 13, but mimicking curve for NGC 253 with a smaller mass nuclear component

four-component model. The rotation of NGC 3079 can be fitted by a similar model. The rotation curves of NGC 253 and IC 342 can be fitted by the same model with a smaller mass nuclear component, as shown in Figures 15 and 16. Rotation curves for the other galaxies can also be reproduced by this model, assuming parameters in between Figures 13 and 16.

In the above fitting to the Miyamoto-Nagai potential with the four mass components, we chose the parameters by trial and error. Even through such a fitting, the parameters (mass and scale radii) can be constrained within an error of ~10%–20%, depending on the quality and resolution of the data. A detailed least-squares fitting to the data would provide us with more realistic sets of parameters.

We have, so far, called the obtained diagrams the "rotation curves." However, they actually mean observed loci of the highest velocity envelopes in the PV diagrams. Non-circular motion, due to a barred potential and density waves, for example, would be superposed on the actual motion of gas, particularly in the central regions. We therefore estimate the deviation of the tangential velocity, represented by the observed PV diagrams along the major axis from that of a circular rotation. Suppose that gas clouds are orbiting on elliptical orbits of eccentricity e. Then, the orbital velocity of a cloud at the perigalactic passage is given by

$$V_0 = V_{\rm rot}(1 + e)^{1/2} , \qquad (5)$$

where $V_{\rm rot}$ is the circular velocity corresponding to the mass distribution as calculated by equation (4). The loci of maximum velocity on the PV diagram will approximate this perigalactic (maximum) orbital velocity.

Therefore, the "rotation curve" may indicate a slightly overestimated circular velocity by a factor of $(1 + e)^{1/2}$. As numerical simulations have shown (Fujimoto & Sørensen 1977; Huntley, Sanders, & Roberts 1978; Noguchi 1988; Wada & Habe 1992), for a highly disturbed orbit of gas in a strong bar shock, the eccentricity is found to be of the order of $e \sim 0.5$. Hence, the apparent rotation velocity from the PV diagrams would only be ~20% higher than a purely circular velocity, even in such an extreme barred-shocked condition. This would, however, result in an overestimation of the mass com-

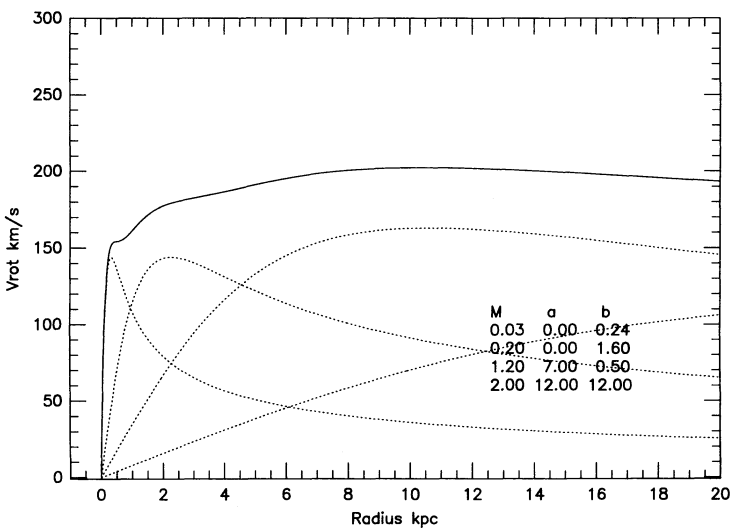

FIG. 16.—Same as Fig. 13, but mimicking curve for IC 342

ponent by a factor of $1 + e$, causing an overestimation of a few tens of percent. Finally, we mention that the rotation of the major gas disk in the central 150 pc of our Galaxy has been shown to be almost circular from a detailed analysis of the CO PV diagrams of Bally et al. (1987) (Sofue 1995).

4. DISCUSSION

We have compiled PV diagrams along the major axes of nearby galaxies, which have been observed in the CO line (central regions), Hα emission (star-forming disk), and in H I lines (disk and outskirts). We used these PV diagrams to obtain total rotation curves from the nuclear region to outskirts. The obtained total rotation curves are shown to be approximately flat from the nuclear region of a few hundred parsecs radius to the outer $R \sim 10$–30 kpc region, except for the inner few hundred parsecs.

A striking feature in the present study is the steeply rising nuclear peak of the rotation curves at $R \sim 100$–200 pc, which is generally observed for all the disk galaxies studied here. This steep rotation peak can be fitted by a mass model in which a compact nuclear mass component of 100–150 pc radius and a mass of several times $10^9\ M_\odot$ is assumed. From a fitting of the observed rotation curves by the Miyamoto-Nagai potential, this nuclear mass component has turned out to be an additional component to the well-known central bulge. Thus, rotation curves of galaxies can generally be fitted by a model with four mass components: the nuclear compact mass, the central bulge, the disk, and the massive halo.

The nuclear mass component would have an essential implication for the formation and evolution of the bulge and the central mass condensation of galaxies, Saio & Yoshii (1990) have shown that the flat rotation curve and exponential-raw mass distribution in disk galaxies are a consequence of a viscous protogalactic disk contraction with ongoing star formation, where the timescales of viscosity and star formation are of the same order, or of the order of the Jeans time of the disk instability. Their model has also produced a central enhancement of the rotation velocity at $R \sim 0.05R_0$ with R_0 being the scale radius of the disk. This is due to a more rapid contraction of the central gas disk compared to the star formation time because of a stronger shearing viscosity in the central disk. The model rotation curves could somehow mimic even the central velocity peak of the observed curves, such as in the Milky Way, NGC 891, and NGC 6946.

However, the model still appears to be unsatisfactory in reproducing, in detail, the steep central peak of rotation curves at $R < \sim 200$ pc corresponding to the compact nuclear mass component. In order for such a compact mass component to appear, a much more rapid contraction of the protogalactic gas disk would have been necessary. Such a rapid contraction of the gas disk prior to star formation might be possible if we could modify (increase) the viscosity in the central gas disk. Alternatively, we may need to take into account a rapid gas accretion through strong galactic shocks in a central oval (bar) potential (Noguchi 1988; Wada & Habe 1992) during the protogalactic disk contraction.

REFERENCES

Bally, J., Stark, A. A., Wilson, R. W., & Henkel, C. 1987, ApJS, 65, 13
Bosma, A. 1981, AJ, 86, 1825
Burton, W. B., & Gordon, M. A. 1978, A&A, 63, 7
Casertano, S. 1983, MNRAS, 203, 735
Casoli, F., Clausset, F., Viallefond, F., Combes, F., & Boulanger, F. 1990, A&A, 233, 357
Clemens, D. P. 1985, ApJ, 295, 422
Combes, F. 1992, ARA&A, 29, 195
Combes, F., Gottesman, S. T., & Weliachew, L. 1977, A&A, 59, 181
Dahlem, M., Salto, S., Klein, U., Booth, R., Mebold, U. Wielebinski, R., & Lesch, H. 1990, A&A, 240, 237
Fujimoto, M., & Sørensen, S. A. 1977, A&A, 60, 251
Garcia-Burillo, S., & Guélin, M. 1995, A&A, in press
Garcia-Burillo, S., Guélin, M., & Cernicharo, J. 1993, A&A, 274, 123
Garcia-Burillo, S., Guélin, M., Cernicharo, J., & Dahlem, M. 1992, A&A, 266, 210
Handa, T., Sofue, Y., Ikeuchi, S., Kawabe, R., & Ishizuki, S. 1992, PASJ, 44, L227
Hayashi, M., Handa, T., Sofue, Y., Nakai, N., Hasegawa, T., Lord, S., & Young, J. 1987, in IAU Symp. 115, Star Forming Regions, ed. M. Peimbert & J. Jugaku (Dordrecht: Reidel), 631
Huntley, J. M., Sanders, R. H., & Roberts, W. W. 1978, ApJ, 221, 521
Irwin, J. A., & Seaquist, E. R. 1991, ApJ, 371, 111
Ishizuki, S., Kawabe, R., Ishiguro, M., Okumura, S. K., Morita, K.-I., Chikada, Y., & Kasuga, T. 1990a, Nature, 344, 224
Ishizuki, S., Kawabe, R., Ishiguro, M., Okumura, S. K., Morita, K.-I., Chikada, Y., Kasuga, T., & Doi, M. 1990b, ApJ, 355, 436
Kenney, J., & Young, S. J. 1988, ApJS, 66, 261
Koribalski, B., Dickey, J. M., & Mebold, U. 1993, ApJ, 402, L41
Malhotra, S. 1994, ApJ, 433, 687
Miyamoto, M., & Nagai, R. 1975, PASJ, 27, 533
Nakai, N., Kuno, N., Handa, T., & Sofue, Y. 1994, PASJ, 46, 527
Noguchi, M. 1988, A&A, 203, 259
Pence, W. D. 1980, ApJ, 239, 54
Rogstad, D. H., & Shostak, G. S. 1972, ApJ, 220, L37
Rots, A. H., Bosma, A., van der Hulst, J. M., Athanassoula, E., & Crane, P. C. 1990, AJ, 100, 387
Rubin, V. C., Ford, W. K., & Thonnard, N. 1980, ApJ, 238, 471
———. 1982, ApJ, 261, 439
Rupen, M. P. 1991, AJ, 102, 48
Sage, L. J., & Solomon, P. M. 1991, ApJ, 380, 392
Saikia, D. J., Unger, S. W., Pedlar, A., Yates, G. J., Axon, D. J., Wolstencroft, R. D., Taylor, K., & Glydenkerne, K. 1990, MNRAS, 245, 397
Saio, H., & Yoshii, Y. 1990, ApJ, 363, 40
Sancisi, R. 1976a, A&A, 53, 159
———. 1976b, in Topics in Interstellar Matter, ed. H. van Woerden (Dordrecht: Reidel), 255
Sandage, A., & Tammann, G. A. 1974, ApJ, 194, 559
Schöniger, F., & Sofue, Y. 1993, A&A, 283, 21
Scoville, N. Z., Soifer, B. T., Neugebauer, G., Young, J. S., Mattheus, K., & Yeka, J. 1985, ApJ, 289, 129
Scoville, N. Z., Thakker, D., Carlstrom, J. E., & Sargent, A. E. 1993, ApJ, 404 L63
Sofue, Y. 1994, PASJ, 46, 173
———. 1995, PASJ, 47, 551
Sofue, Y., Doi, M., Ishizuki, S., Nakai, N., & Handa, T. 1988, PASJ, 40, 511
Sofue, Y., Honma, M., & Arimoto, N. 1994, A&A, 296, 33
Sofue, Y., & Irwin, J. 1992, PASJ, 44, 353
Sofue, Y., & Nakai, N. 1993, PASJ, 45, 139
———. 1994, PASJ, 46, 147
Stark, A. A., & Brand, J. 1989, ApJ, 339, 763
Tacconi, L. J., & Young, J. S. 1986, ApJ, 308, 600
Tully, R. B. 1974, ApJS, 27, 437
———. 1988, Nearby Galaxy Catalogue (Cambridge: Cambridge Univ. Press)
Véron-Cetty, M.-P., & Véron P. 1985, A&A, 145, 425
Wada, K., & Habe, A. 1992, MNRAS, 258, 82
Young, J. S., Claussen, M. J., & Scoville, N. Z. 1988, ApJ, 324, 115
Young, J. S., & Scoville, N. Z. 1982, ApJ, 258, 467
———. 1992, ARA&A, 29, 581